# Ideal MHD Stability of a Spherical Tokamak Power Plant and a Component Test Facility

**M. J. Hole,[1] H. R. Wilson,[2] R. Abeysuriya,[1,3] and J. W. Larson[1,4,5]**

[1] Research School of Physical Sciences and Engineering, Australian National University, Acton 0200, ACT Australia

[2] Department of Physics, University of York, Heslington, York Y010 5DD, UK

[3] School of Physics, University of Sydney 2006, NSW Australia

[4] Mathematics and Computer Science Division, Argonne National Laboratory, 9700 S. Cass Avenue, Argonne, IL 60439 USA

[5] Computation Institute, University of Chicago, 5735 S. Ellis Avenue, Chicago, IL 60637 USA

**Abstract.** We have investigated ideal MHD stability of two advanced spherical tokamak confinement concepts: the Spherical Tokamak Power Plant, a 3 GW concept fusion power plasma producing 1 GW of electric power, and the Component Test Facility, a concept designed for in situ materials testing for ITER and beyond. Detailed stability studies for toroidal mode number $n = 1, 2, 3$ displacements are presented as a function of conformal wall radius $R_w$ and on-axis safety factor $q_0$. These confirm that both concepts are stable provided that the wall is sufficiently close and $q_0$ sufficiently large ($q_0 > 2.8$ for the power plant and $q_0 > 2.1$ for the component test facility). For the component test facility we have also extended earlier scans to study the marginal stability boundaries for constant plasma current $I_p$. This work involved implementing parallel versions of the equilibrium transformation and stability scans. Both power plant and component test facility configurations are found to be ballooning stable.

PACS numbers: 52.55.Fa, 52.55.-s,52.55.Tn,28.52.-s

Submitted to: *Plasma Phys. Control. Fusion*

## 1. Introduction

As well as complementing the physics base for ITER [1], theory and progress in spherical tokamak experiments have prompted design studies into thermonuclear fusion facilities having a tight aspect ratio: the component test facility [2, 3] and spherical tokamak power plants [4, 5, 6]. A UK Component Test Facility (CTF) concept is an aspect ratio $A = R/a = 0.75/0.47 = 1.60$ spherical tokamak with moderate elongation $\kappa = 2.7$, with 8.0 MA of plasma current $I_p$ and 10.5 MA of toroidal field rod current. The machine, which is designed for in situ materials testing in parallel with ITER and beyond, provides a test area of $\approx 10$ m$^2$ with a projected 14 MeV neutron flux of 1-2 MW m$^{-2}$ [7]. Voss et al. [2] give a detailed study of vertical plasma stability, neutronics, and engineering. A larger, alternative design, extrapolated based on the stable operating space of the NSTX concept, has also been developed by Peng et al. [3] and Stambaugh et al. [8].

More comprehensive MHD stability scans have been conducted on the more challenging Spherical Tokamak Power Plant (STPP) [6]. This 3 GW fusion power plant concept, designed to deliver 1 GW electric power, has an aspect ratio $A = R/a = 3.42/2.44 = 1.40$, $I_p = 31$ MA, and 30.2 MA of centre rod current. Preliminary MHD studies have shown that stable configurations can be produced provided that the wall is sufficiently close and the on-axis safety factor $q_0$ is sufficiently large [6]. Detailed studies have been conducted on other similar designs, such as the ARIES-ST configuration [5, 9]. Some relevant parameters for the STPP [6] and CTF [2] designs that we analyse in this paper are listed in Table 1. We focus attention on the stability of ideal MHD modes with toroidal mode number $n = 1, 2, 3$, as well as $n = \infty$ ballooning modes. Vertical ($n = 0$) stability has been treated by a separate study using the PACE [10] filament code. For both the CTF and STPP concepts, stability scans are performed as a function of safety factor $q$ and wall position. For the CTF concept, which has parameters much closer to present day experiments, we have also investigated stability as a function of $q$ with fixed $I_p$.

This paper is structured as follows: Sections 2 and 3 present analysis of the MHD

**Table 1.** Selection of parameters for the STPP [6] and CTF [2] baseline designs.

| Quantity | Description | STPP | CTF |
|---|---|---|---|
| R/a | major/minor radius (m) | 3.42/2.44 | 0.75/0.47 |
| $\kappa, \delta$ | elongation, triangularity | 3.2, 0.55 | 2.7,0.3 |
| $I_p$ | plasma current (MA) | 31 | 8 |
| $I_{BS}/I_p$ | bootstrap fraction (%) | 92.6 | 41 |
| $q_0$,$q_a$ | axis, edge safety factors | 3,15 | 2.2, 6.2 |
| $\beta_{exp}$,$\beta_n$ | beta (%), normalized beta | 59,8.2 | 20, 3.4 |
| $l_i^{(2)}$ | internal inductance | 0.21 | 0.53 |

stability of the STPP and the CTF, respectively. These stability analyses are based on a SCENE [11] Grad-Shafranov equilibrium produced on a $(R, Z)$ mesh. Ideal MHD stability is investigated with the KINX stability code [12], described in Sec. 3, and uses the CAXE [13] equilibrium code to remap the equilibrium from SCENE. For the CTF studies the equilibrium code CHEASE [14] was used to modify the configuration when performing detailed stability studies as a function of $q$ with fixed $I_p$. We close in Sec. 4 with some concluding remarks.

## 2. Stability of the Spherical Tokamak Power Plant

To demonstrate convergence of the equilibrium and subsequent MHD stability studies, a scan was performed of both global equilibrium properties and the MHD growth rate with increasing grid resolution. A high spatial resolution (169 radial by 257 axial grid point) SCENE equilibrium is shown in Fig. 1. Figure 1(a) shows contours of constant poloidal flux $\psi$, and 1(b) shows the $\psi$ variation along the mid-plane ($Z = 0$). The figures reveal the large Shafranov shift for this equilibrium. Figures 1(c) through 1(g) respectively show the assumed profiles of $q(\psi)$, pressure $p(\psi)$, toroidal flux function $f(\psi) = RB_\phi$, and the derivatives $p'(\psi)$ and $f(\psi)f'(\psi)$ used to constrain the grad-Shafranov equation. Note that SCENE calculates the $f(\psi)$ profile that is consistent with $p(\psi)$, the bootstrap current and driven current profile.

Using the plasma boundary $p'(\psi)$ and $f(\psi)f'(\psi)$ profiles from SCENE, we generated

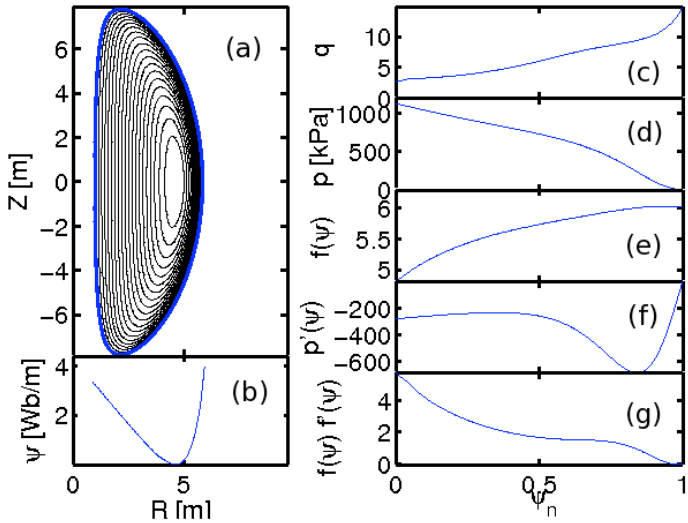


**Figure 1.** Spherical Tokamak Power Plant (STPP) equilibrium. Figure 1 (a) is a contour map of equal spaced $\psi_n$, and the blue contour is the plasma boundary. Figure 1 (b) shows the poloidal flux through the mid-plane $Z = 0$. Figures 1 (c) through 1 (g) show the $q$, pressure $p(\psi)$, toroidal flux function $f(\psi)$, and $p'(\psi)$ and $f(\psi)f'(\psi)$ profiles, respectively.

CAXE equilibrium solutions of increasing grid resolution from $N = N_\psi = N_\theta = 16$ to $N = 160$ grid points. Here, $N_\psi$ and $N_\theta$ are the number of radial and poloidal grid points. For each grid resolution, the solution was iterated until the variation of magnetic surfaces, $\varepsilon_{level}$, was less than $10^{-5}$, and the change in normalised radius $\rho$ between subsequent iterations, $\varepsilon_\rho$, was less than $10^{-5}$. Figure 2 shows the variation in global quantities with increasing $N$ of (a) the plasma internal inductance $l_i$ and (b) the normalized beta $\beta_n$. The figure shows that the volume integrated quantities have converged in the interval $100 < N < 140$.

With the equilibrium described, ideal MHD stability can be examined. First, in the absence of a vacuum (*i.e.* a conducting wall on the plasma surface) and for each CAXE equilibrium solution, the most unstable $n = 1, 2, 3$ modes were found using KINX. Figure 2(c) shows the variation in normalized growth rate $\omega^2/\omega_A^2$ of the most unstable solution as a function of $1/N^2$ for the different $n$ eigenmodes. Here, $\omega_A$ denotes the on-axis Alfvén frequency at the geometric axis, calculated in vacuo. In this analysis a flat density profile was used. For $n = 1, 2$ convergence is approximately linear, with

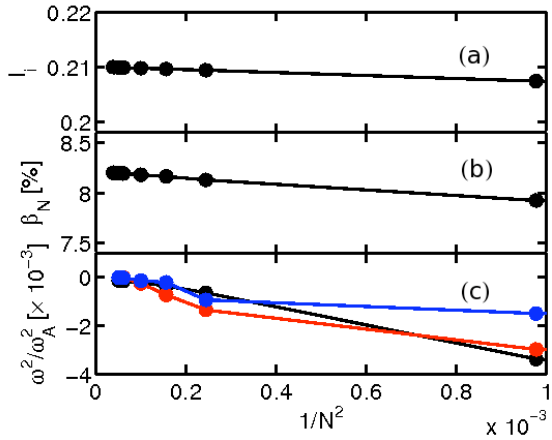


**Figure 2.** Integrated quantities of the STPP equilibrium versus grid dimensions $N$: Figure 2 (a) is the CAXE internal inductance $l_i$, Figure 2 (b) shows the CAXE $\beta_n$ value, and Figure 2 (c) shows most unstable eigenvalue for $n = 1$ (black), $n = 2$ (blue), $n = 3$ (red).

$1/N^2$ over the range $10^{-4} < 1/N^2 < 10^{-3}$, in agreement with earlier convergence studies for less demanding equilibria [12]. For the remaining analysis in this work, a value of $N = 128$ was used to investigate stability limits. The same grid resolution has been used previously to study ideal MHD limits in the MAST spherical tokamak [15].

Two free scalings of the equilibrium are available, which can be used to generate families of solutions to the grad-Shafranov equation from a single solution. These transformations can be combined to provide for a change in either $I_p$ or $q$ at a prescribed poloidal flux surface [14]. We have used this freedom to investigate the internal stability as a function of $q_0$, with a conducting wall at the plasma boundary. Figure 3 shows the normalized eigenvalue for different $q_0$ values with $N = 128$. The $q_0$ scan reveals that the plasma is stable for $q_0 \geq 2.8$ but unstable to the axis-asymmetric modes for $q_0 < 2.8$. Projection of the eigenfunction for an unstable configuration ($q_0 = 2.5$) confirms the internal nature of the mode. Figure 4(a) and 4(c) respectively show a selection of poloidal harmonics and the normal mode displacement for an $n = 1$ mode versus the square root of normalized flux, $s = \sqrt{\psi_n}$. The low dominant poloidal mode numbers suggest a resonance with the core where $q$ is small.

The addition of a vacuum region allows the edge displacement to be nonzero at the

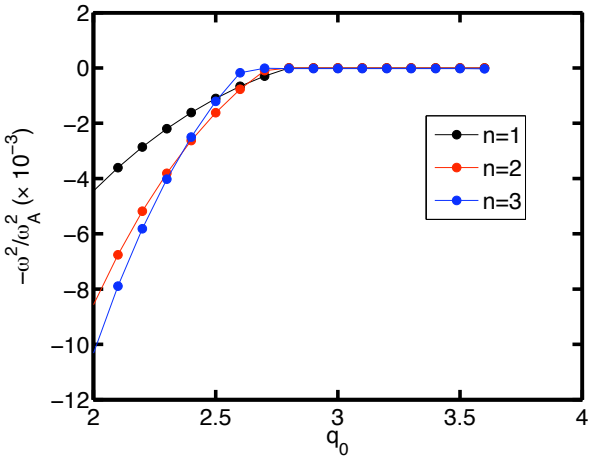


**Figure 3.** Scan of eigenvalue versus $q_0$ for the STPP equilibrium with no vacuum conducting wall at plasma boundary.

plasma boundary. Thus, gradients in the current density or pressure near the edge of the plasma couple more strongly to the displacement and increase the drive. For example, Figure 4 (b) shows a selection of poloidal harmonics and Figure 4 (d) the normal mode displacement of an $n = 1$ mode with equilibrium $q_0 = 2.9$ and $R_w/a = 1.3$ The spatial projection of the eigenfunction shows the mode becoming more localized to the vertical extremities of the plasma.

We also conducted a stability scan of the low $n$ modes as a function of wall position. The perfectly conducting wall was selected to be conformal to the plasma boundary. Figure 5 shows the normalized eigenvalue $\omega^2/\omega_A^2$ for $n = 1, 2, 3$ as a function of the wall parameter $R_w/a$. The scans show that the plasma is stabilised with respect to the external $n = 1, 2, 3$ modes provided $R_w/a < 1.15$.

The STPP was designed to be second stable to ballooning modes across the entire minor radius [6]. We have confirmed ballooning stability using the ballooning code BALM2000 [16], and Figure 6 shows the maximum achievable pressure gradient versus the square root of normalized flux. As with the MAST calculations [15], we have chosen the numerical integration interval over the poloidally extended "ballooning" angle to be 20 periods, while the initial angle (*i.e.* that about which the mode balloons) was chosen to be zero.

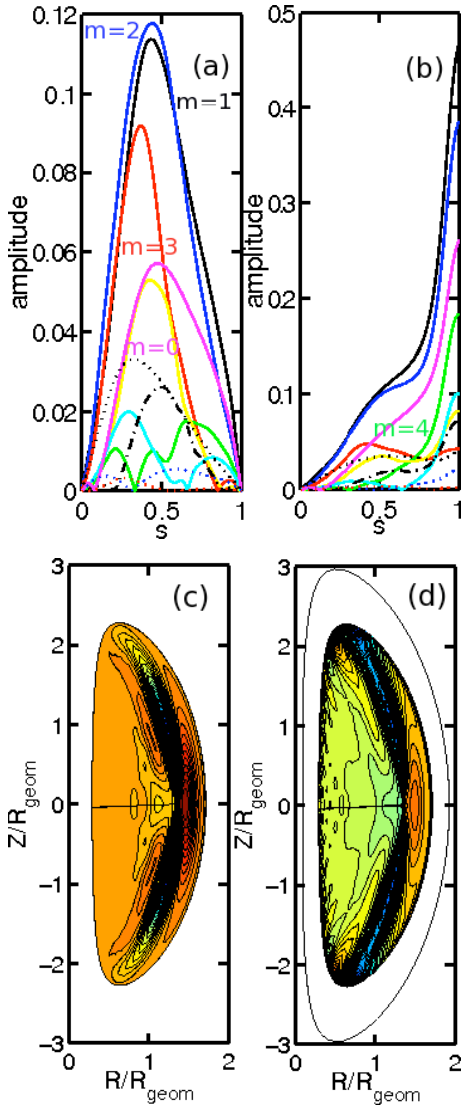


**Figure 4.** STPP eigenfunctions of $n = 1$ marginally unstable displacements for (a) and (c) an internal mode with $R_w/a = 1$ and $q_0 = 2.5$, and (b) and (d) an external mode with $R_w/a = 1.2$ and $q_0 = 2.9$. Figures 4 (a) and 4 (b) show the $s$ profile of selected harmonics, and Figures 4 (c) and 4 (d) show the full eigenfunction displacements. The colormap is a sliding jet colorbar, where red corresponds to an expansion, and blue a contraction in the direction normal to the contour.

## 3. Component Test Facility

In this section we report on more detailed scans that augment earlier studies of vertical MHD stability. [2] Specifically, we have conducted marginal stability scans over the total beta $\overline{\beta} = 2\overline{p}/\overline{B^2}$, where the overline denotes the volume average, by extending the equilibrium remapping of the surface averaged current $I^*(s)$ to preserve both the plasma current $I_p$ and $q_0$ at fixed $\overline{\beta}$. The total beta $\overline{\beta}$ is related to the experimental beta, $\beta_{exp}$,

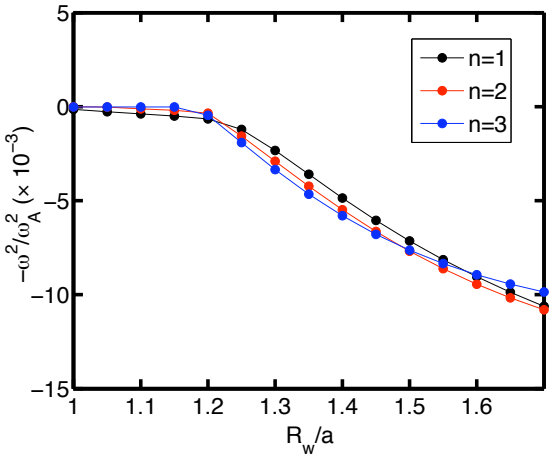


**Figure 5.** Normalized eigenvalue versus wall parameter $R_w/a$ for $n = 1, 2, 3$ eigenmodes of the STPP equilibrium.

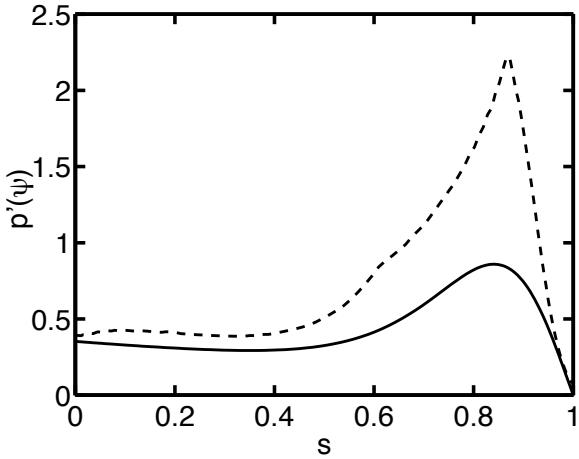


**Figure 6.** Ballooning stability of the STPP equilibrium. The solid line is the pressure gradient profile of the STPP equilibrium, and the dashed line is the marginally stable threshold.

through $\beta/\overline{\beta} = \overline{B^2}/B_0^2$, where $B_0$ is the vacuum toroidal field at the geometric axis. We have used the equilibrium code CHEASE [14] to remap for the surface averaged current $I^*(s)$. Two equilibrium remappings for $I^*(s)$ were explored:

$$I^*(s) = \lambda_1 I^*(s^{\lambda_2}), \tag{1}$$

$$I^*(s) = \lambda_1 (I^*(s) + \lambda_2 I^*(0)(1-s)), \tag{2}$$

with $\lambda_1, \lambda_2$ adjusted to preserve $I_p$ and $q_0$ for each new target $\overline{\beta}$, where $I^*(0)$ is the value of the unmapped $I^*(s)$ at $s = 0$. In both remappings of Eq. (1) and Eq. (2), automated

equilibrium scans were performed by using task-parallel Python scripts. These scripts were constructed using the PyPar [17] Python bindings to the Message Passing Interface library. The calculations were executed on a local commodity cluster. First, these scaled $p'$ to achieve a target $\overline{\beta}$. Next, an interpolative search algorithm was used to adjust $\lambda_2$ to obtain the original $q_0$ value. For each $\lambda_2$ value, $\lambda_1$ was automatically adjusted within CHEASE to preserve $I_p$. Because of parameter interdependency, this process was iterated until all three parameters converged.

Figure 7 shows contours of constant $\overline{\beta}$ in $(q_0, \lambda_2)$ space with constant $I_p$. As the purpose of this figure is to identify the effect of automated equilibrium remappings of Eq. (1) and Eq. (2) on $q_0$, we have restricted our attention to a parameter range for which $q_0$ is monotonic with $\lambda_2$. For both remappings, $q_0$ drops with increasing $\overline{\beta}$ at fixed $\lambda_2$, and $q_0$ decreases with increasing $\lambda_2$ at fixed $\overline{\beta}$. The latter trend corresponds to adding current to the plasma core: the nonlinear mapping of Eq. (1) corresponds to an inward contraction of the current profile, while the remapping of Eq. (2) corresponds to adding on-axis current $I^*(0)$. We have selected remapping Eq. (2) for use in marginal stability scans because this accesses higher $\overline{\beta}$ for the baseline $q_0$.

Figure 8 shows a CHEASE computed equilibrium of the CTF configuration, using input parameters from SCENE. While not shown here, we have performed similar equilibrium and stability convergence studies to those described in Sec. 2 for the STPP. Also shown in Figures 8(c) and (g) are the $q$ and $I^*(s)$ profile variation using the application of Eq. (2) with $I_p$ and $q_0$ preserved for $0.06 < \overline{\beta} < 0.15$. Over this range of $\overline{\beta}$, the change in the $I^*(s)$ profile is less than 5%, even at the core where the modification is largest. This explains why the variation in $q$ and $I^*(s)$ is barely visible. Figure 8(d) shows the corresponding variation of pressure profile over this range of $\overline{\beta}$, and with $I_p$ and $q_0$ preserved.

We have investigated stability as a function of conformal wall radius and $q_0$. For $R_w/a < 2.2$ the plasma is stable to $n = 1$ displacements, and it is stable to $n = 2$ and $n = 3$ displacements in the no wall limit. Figure 9 shows the change in plasma

stability as a function of $q_0$ with a conducting wall on the plasma boundary. While the plasma current was not conserved in these scans, they show nonetheless that the plasma is stable to $n = 1, 2$ and 3 internal modes provided $q_0 > 2.1$. As illustration, Fig. 10 shows $n = 1$ eigenfunctions for external (no-wall) and internal (wall on boundary) kink modes for $q_0 = 2.1$. The substantial $m = 2$ lobes indicate a resonance with the $q = 2$ surface.

Using the equilibrium transformation of Eq. (2), we have also computed more detailed marginal stability boundaries in $(R_w/a, \overline{\beta})$ parameter space. For instance, Fig.

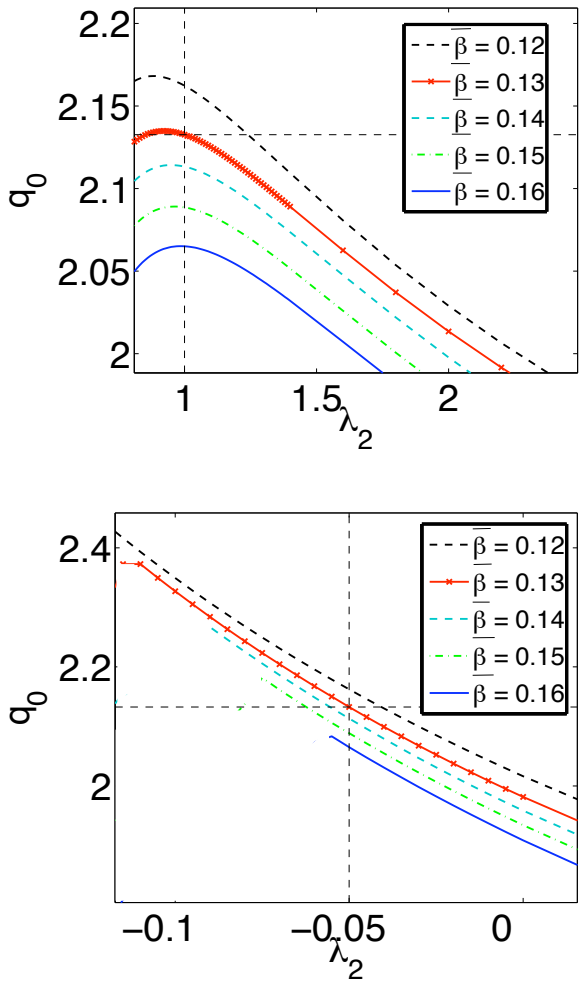


**Figure 7.** Scaling of $q_0$ versus $\lambda_2$ for the equilibrium transformations useded for the Component Test Facility. Figure 7 (a) is the nonlinear flux surface rescaling of Eq. (1), and Figure 7 (b) shows the addition of an on-axis current given by Eq, (2). Intersections of $\overline{\beta}$ contours with the horizontal dashed line are solutions for $\lambda_2$ that preserve $q_0$.

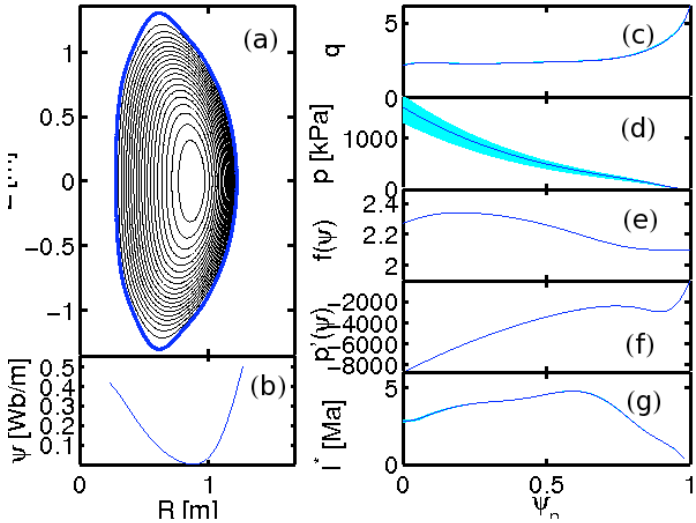


**Figure 8.** Component Test Facility equilibrium. Figure 8 (a) is a contour map of equal-spaced $\psi_n$, and the blue contour is the plasma boundary. Figure 8 (b) shows the poloidal flux through the mid-plane $Z = 0$. Figures 8 (c) through 8 (g) show the $q$ profile, pressure $p(\psi)$, toroidal flux function $f(\psi)$, and $p'(\psi)$ and $I^*$ profiles respectively. The light shading in Figures 8 (c), 8 (d) and 8 (g) represents the variation of the $q$, $p$, and $I^*$ for the marginal stability scans performed.

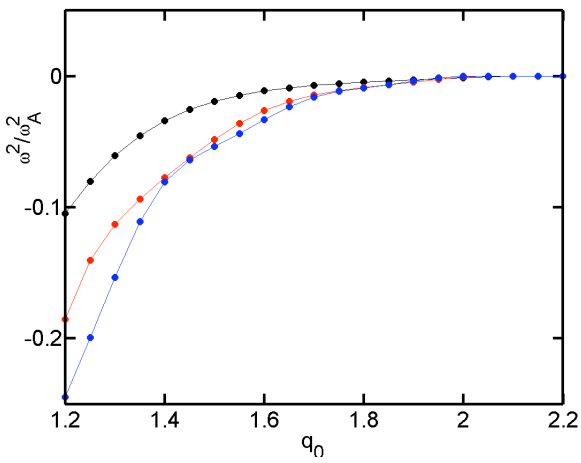


**Figure 9.** Change in plasma stability for the CTF equilibrium as a function of $q_0$.

11 shows the $(R_w/a, \overline{\beta})$ marginal stability boundary for $n = 1$ displacements for constant $q_0$ and $I_p$, and constant $q_0$ only. Also shown is the $(R_w/a, \overline{\beta})$ marginal stability boundary for constant $I_p$. As expected, the maximum $\overline{\beta}$ increases with decreasing wall distance. The change in stability at $\overline{\beta} = 0.14$ occurs because the $q$ profile becomes non-monotonic, so the zero shear surface moves off-axis with increasing $\overline{\beta}$, into regions of the plasma for which the destabilising pressure and current gradients are larger. Also shown is the

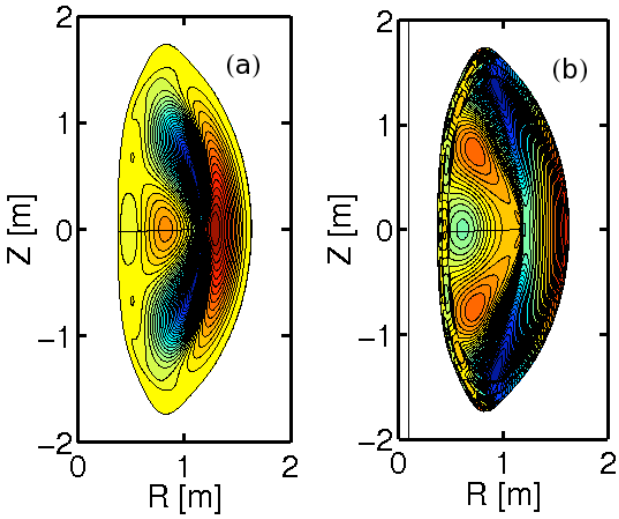


**Figure 10.** CTF mode structure of an $n = 1$ displacement for an (a) internal (wall on plasma) and (b) external (wall at infinity) mode.

marginal stability boundary when only $q_0$ is preserved and $I_p$ is unconstrained. For this curve $I_p$ is 8.0 MA between $0.114 < \overline{\beta} < 0.13$, $I_p$ drops to 7.6 MA at $\overline{\beta} = 0.15$, and $I_p$ increases to 11.1 MA at $\overline{\beta} = 0.06$. This trend explains both the improved performance for $\overline{\beta} > 0.135$, as the current gradient is weaker in this case compared to the boundary with both $I_p$ and $q_0$ preserved, and the reduced performance compared to the fixed $I_p$ case for $\overline{\beta} < 0.115$, for which the current gradient is larger.

Figure 12 is a contour plot showing the available increase in maximum possible pressure gradient, $\Delta p'(\psi)$, such that the plasma is ballooning stable. This shows that there is considerable margin before the onset of ballooning instability. As in Sec. 2 we have checked that the ballooning stability conclusions are insensitive to the initial angle and the number of periods of integration.

## 4. Conclusions

We have performed an ideal MHD stability analysis on high-resolution equilibrium reconstructions for the spherical tokamak power plant and component test facility configurations. An equilibrium and MHD stability convergence study was performed, showing convergence of both globally integrated quantities and MHD eigenvalues. Taken

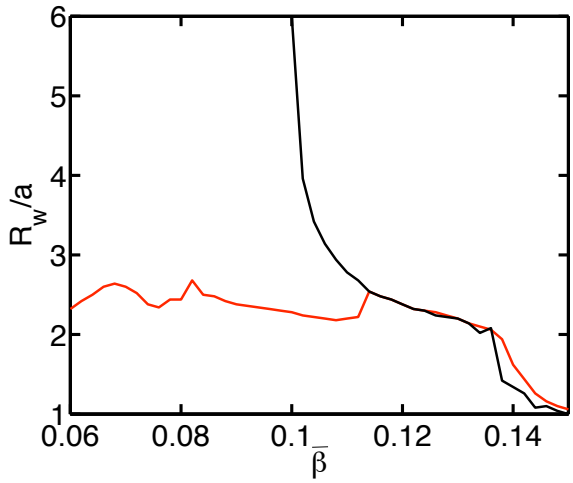


**Figure 11.** Marginal $n = 1$ stability boundary in $(R_w/a, \overline{\beta})$ space for the CTF configuration. The black line shows the marginal stability boundary using the $I^*$ mapping of Eq. (2) with both $I_p$ and $q_0$ preserved, and the red line shows the marginal stability boundary with only $q_0$ preserved. In each case the plasma is more stable below the curve (lower value of $R_w/a$), and unstable above the curve (larger value of $R_w/a$). The baseline $\overline{\beta}$ value is 0.13.

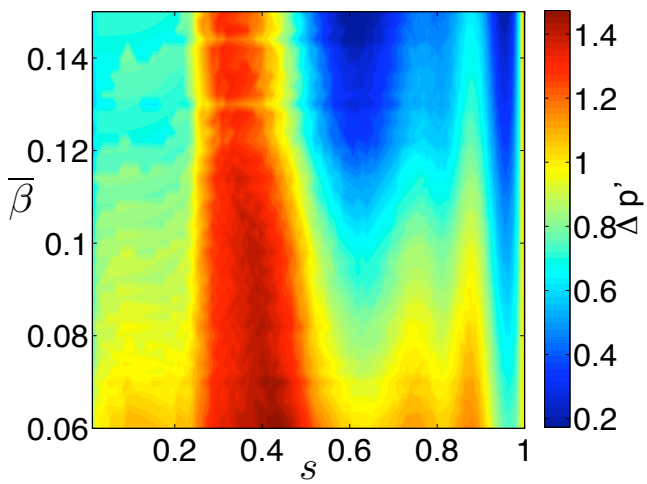


**Figure 12.** Contour plot of ballooning mode maximum increase in pressure gradient $\Delta p'(\psi)$ for the CTF configuration as a function of $s$ and $\overline{\beta}$.

together, these results confirm the existence of stable, high-performance configurations in the spherical tokamak family.

For the power plant, the central conclusions are threefold. First, of the axis-asymmetric modes investigated ($n = 1, 2, 3$), a scan with $q_0$ shows that the equilibrium is stable to internal modes provided $q_0 > 2.8$. Second, a stability scan with an ideal

conformal wall showed that the low $n$ modes ($n = 1, 2, 3$) are stabilised provided $R_w/a < 1.15$. Three, the power plant equilibrium is stable to $n = \infty$ ballooning modes.

We have also explored the stability of a component test facility configuration as a function of $q_0$, $R_w/a$ and $\overline{\beta}$ for constant $I_p$ and $q_0$. Specifically, we find: the configuration is stable to $n = 1, 2, 3$ internal modes provided $q_0 > 2.1$; the $n = 1$ external kink mode is stabilised provided $R_w/a \leq 2.2$, and the plasma is $n = \infty$ ballooning stable. We find that there is a considerable stable operating $\overline{\beta}$ margin with respect to ballooning modes: the plasma is ballooning stable up to at least $\overline{\beta} = 0.15$; and for a tightly fitting wall, the plasma is $n = 1$ stable up to $\overline{\beta} = 0.15$ ($\beta_{exp} = 23\%$).

## Acknowledgments

We thank O. Sauter and H. Lujtens for their support and technical assistance in the operation of the CHEASE equilibrium code, S. Medvedev in the operation of the KINX stability code, and Ole Nielsen in the installation and usage of PyPar. This work was partly funded by the Australian Research Council through grant FT0991899, the United Kingdom Engineering and Physical Sciences Research Council, and Argonne National Laboratory operated by UChicago Argonne LLC for the United States Department of Energy under contract DE-AC02-06CH11357.

## References

[1] M. Gryaznevich, R. J. Akers, G. F. Counsell, G. Cunningham, A. Dnestrovskij, A. R. Field, T. C. Hender, A. Kirk, B. Lloyd, H. Meyer, A. W. Morris, A. Sykes, A. Tabasso, M. Valovic, G. M. Voss, H. R. Wilson, , MAST, and NBI teams. Next step targeted experiments on the Mega-Amp Spherical Tomakak. *Phys. Plas.*, 10(5):1803–1808, 2003.

[2] G. M. Voss, S. Davis, A. Dnestrovskij, A. Kirk, P. J. Knight, M. Loughlin, M. H. O'Brien, D. Sychugov, A. Tabasso, and H. R. Wilson. Conceptual deisgn of a component test facility based on the spherical tokamak. *Fus. Eng. and Des.*, 83:1648–1653, 2008.

[3] Y-K M. Peng, P. J. Fogarty, T. W. Burgess, D. J. Strickler, B. E. Nelson, J. Tsai, C. A. Neumeyer, R. Bell, C. Kessel, J. Menard, D. Gates, B. LeBlanc, D. Mikkelsen, E. Fredrickson, L. Grisham,

J. Schmidt, P. Rutherford, S. Sabbagh, A. Field, A. Sykes, I. Cook, O. Mitarai, and Y. Takase. A component test facility based on the spherical tokamak. *Plas. Phys. Con. Fus.*, 47:B263–B283, 2005.

[4] R.J. Akers, A. Bond, R.J. Buttery, P.G. Carolan, G.F. Counsell, G. Cunningham, S.J. Fielding, C.G. Gimblett, M. Gryaznevich, R.J. Hastie, P. Helander, T.C. Hender, P.J. Knight, C.N. Lashmore-Davies, G.P. Maddison, T.J. Martin, K.G. McClements, A.W. Morris, M.R.O'Brien, C. Ribeiro, C.M. Roach, D.C. Robinson, A. Sykes, G.M. Voss, M.J. Walsha, H.R. Wilson, and F.S. Zaitsev. Steady state operation of spherical tokamaks. *Nuc. Fus.*, 40(6):1223–1244, 2000.

[5] F. Najmabadi. Spherical torus concept as power plants - the ARIES-ST study. *Fus. Eng. Des.*, 65(2), 2003.

[6] H. R. Wilson, J.-W. Ahn, R.J. Akers, D. Applegate, R.A. Cairns, J.P. Christiansen, J.W. Connor, G. Counsell, A. Dnestrovskij, W.D. Dorland, M.J. Hole, N. Joiner, A. Kirk, P.J. Knight, C.N. Lashmore-Davies, K.G. McClements, D.E. McGregor, M.R. O'Brien, C.M. Roach, S. Tsaun, and G.M. Voss. Integrated plasma physics modelling for the Culham steady state spherical tokamak fusion power plant. *Nuc. Fus.*, 44:917–929, 2004.

[7] A. W. Morris, R. J. Akers, G. F. Counsell, T. C. Hender, B. Lloyd, A. Sykes, G. M. Voss, and H. R. Wilson. Spherical tokamaks: Present status and role in the development of fusion power. *Fus. Eng. and Des.*, 74:67–75, 2005.

[8] R. D. Stambaugh, V. S. Chan, C. P. C. Wong, J. P. Smith, A. M. Garofalo, and J. A. Leuer. Candidates for a Fusion Nuclear Science Facility (FDF and ST-CTF). In *37th European Physical Society Conference on Plasma Physics and Controlled Fusion*, Dublin, Ireland, June 2010.

[9] S. C. Jardin, C. E. Kessel, J. Menard, T. K. Mau, R. Miller, F. Najmabadi, V. S. Chan, L. L. Lao, Y. R. Linliu, R. L. Miller, T. Petrie, P. A. Politzer, and A. D. Turnbull. Physics basis for a spherical torus power plant. *Fus. Eng. Des.*, 65:165–197, 2003.

[10] P. J. Knight, M. Cox, and T. C. Hender. A filament code for tokamak axisymmetric stability. *Comp. Phys. Comm.*, 71:99, 1992.

[11] H. R. Wilson *et al.* SCENE bootstrap current model upgrade to the full Hirshman-Sigmar formulation for thermal species, with modifications to allow for anisotropic pressure: SCENE4.0. Technical Report 29.1, UKAEA Fusion, 1996.

[12] L. Degtyarev, A. Martynova, S . Medvedev, E. Troyon, L . ViUard, and R. Gruber. The KINX ideal MHD stability code for axisymmetric plasmas with separatrix. *Comp. Phys. Comm.*, 103:10–27, 1997.

[13] S. Medvedev, L. Villard, L. M. Degtyarev, A. Martynov, R. Gruber, and F. Troyon. MHD equilibrium and stability of Doublet configurations. In *Proc. 20th EPS Conference on Controlled*

*Fusion and Plasma Physics,* volume 17C, pages 1279–1282, July 1993.

[14] H. Lutjens, A. Bondeson, and O. Sauter. The CHEASE code toroidal MHD equilibria. *Comp. Phys. Comm.*, 97:219–260, 1996.

[15] M.J. Hole, R.J. Akers, L.C. Appel, R.J. Buttery, C. Brickley, N.J. Conway, M. Gryaznevich, T.C. Hender, O.J. Kwon, M. Valovic, S. Medvedev, A. Patel, S. Saarelma, D. Taylor, H.R. Wilson, and the MAST Team. Ideal MHD stability of the mega-ampere spherical tokamak. *Plasma Phys. Controlled Fusion*, 47:581–613, 2005.

[16] P. N. Vabishchevich, L. M. Degtyarev, and S. Yu Medvedev. Limiting $\beta$ set by ballooning instabilities in a tokamak. *Sov. J. Plas. Phys.*, 9(1):100–104, 1983.

[17] Ole Nielsen. pyPar Google Code Site. http://code.google.com/p/pypar/, 2010.

**LICENSE**

The submitted manuscript has been created by UChicago Argonne, LLC, Operator of Argonne National Laboratory ("Argonne"). Argonne, a U.S. Department of Energy Office of Science laboratory, is operated under Contract No. DE-AC02-06CH11357. The U.S. Government retains for itself, and others acting on its behalf, a paid-up nonexclusive, irrevocable worldwide license in said article to reproduce, prepare derivative works, distribute copies to the public, and perform publicly and display publicly, by or on behalf of the Government.